










Hydroxylated Mg-rich Amorphous Silicates: A New Component of the 3.2 μm Absorption Band of Comet 67P/Churyumov–Gerasimenko

V. Mennella¹ , M. Ciarniello² , A. Raponi² , F. Capaccioni², G. Filacchione² , T. Suhasaria¹, C. Popa¹, D. Kappel^{3,4} , L. Moroz⁴, V. Vinogradoff⁵ , A. Pommerol⁶, B. Rousseau², I. Istiqomah⁷, D. Bockelee-Morvan⁸, R. W. Carlson⁹, and C. Pilorget¹⁰ 

¹ INAF—Osservatorio Astronomico di Capodimonte, via Moiariello 16, I-80131 Napoli, Italy; vito.mennella@inaf.it

² IAPS–INAF, Istituto di Astrofisica e Planetologia Spaziali, Area di Ricerca di Tor Vergata, Via del Fosso del Cavaliere, 100, I-00133 Rome, Italy

³ Institute of Physics and Astronomy, University of Potsdam, Karl-Liebknecht-Str. 24-25, D-14476 Potsdam, Germany

⁴ Institute for Planetary Research, German Aerospace Center (DLR), Rutherfordstr. 2, D-12489 Berlin, Germany

⁵ Aix-Marseille Université, Physique des Interactions Ioniques et Moléculaires PIIM UMR CNRS, 7345, Avenue Escadrille Normandie-Niemen, F-13397 Marseille Cedex 20, France

⁶ Physikalisches Institut, Sidlerstrasse 5, University of Bern, CH-3012 Bern, Switzerland

⁷ Université Grenoble Alpes, CNRS, IPAG, F-38000 Grenoble, France

⁸ LESIA, Observatoire de Paris, PSL Research University, CNRS, Sorbonne Université, Université Paris Diderot, Sorbonne Paris Cité, 5 place Jules Janssen, F-92195 Meudon, France

⁹ Jet Propulsion Laboratory, California Institute of Technology, Pasadena, CA 91109, USA

¹⁰ Institut d'Astrophysique Spatiale, Université Paris Sud, Orsay, France

Received 2020 February 19; revised 2020 April 29; accepted 2020 May 9; published 2020 July 14

Abstract

The VIRTIS imaging spectrometer on board Rosetta has shown that the nucleus surface of comet 67P/Churyumov–Gerasimenko (67P/CG) is characterized by a broad absorption band at around 3.2 μm . The feature is ubiquitous across the surface and its attribution to (a) specific material(s) has been challenging. In the present Letter, we report an experimental investigation showing that the interaction of hydrogen atoms with Mg-rich amorphous silicates determines the formation of hydroxyl groups. The resulting IR spectrum exhibits a broad feature around 3.2 μm similar to that of comet 67P/CG. Hapke's radiative transfer model was employed to estimate an upper limit contribution of 65% of hydroxylated silicates to the observed cometary band intensity. The presence of a hydroxylated fraction in silicates on the cometary surface would represent an evolutionary link between primitive objects of the solar system and dust in the interstellar medium (ISM), where silicate grains can be hydroxylated after having interacted with hydrogen atoms. This link is consistent with the detection of the aliphatic organics in 67P/CG that also originate in the ISM.

Unified Astronomy Thesaurus concepts: [Astrochemistry \(75\)](#); [Comets \(280\)](#); [Laboratory astrophysics \(2004\)](#)

1. Introduction

The payload instruments on board ESA's Rosetta mission have observed the evolution of the Jupiter-family comet 67P/Churyumov–Gerasimenko (67P/CG) in a period from 2014 August to 2016 September and encompassing the perihelion passage occurring in 2015 August at a heliocentric distance of 1.24 au. The data collected have provided unprecedented spatial, spectral, and temporal coverage of the changes occurring on a cometary surface and surrounding inner coma before, during, and after perihelion passage (Taylor et al. 2017). Determining the nucleus surface composition was one of the primary scientific objectives of the Visible, Infrared and Thermal Imaging Spectrometer (VIRTIS; Coradini et al. 2007).

When observed at the global scale, the 67P/CG surface appears dominated by a dust layer, remarkably uniform in composition. The overall spectral reflectance is characterized by a low albedo (0.06) and red slope at visible wavelengths, while a wide absorption band centered at 3.2 μm is a distinctive feature in the infrared range (Capaccioni et al. 2015; Ciarniello et al. 2015). Temporal and spatial spectral variability at the global scale has been observed on the 67P/CG surface (Ciarniello et al. 2016) in addition to spatial variations on meter scales where color changes have been correlated with surface composition inhomogeneities and active sources (Filacchione et al. 2019). In particular, local water ice enrichments show higher albedo and flatter-to-blue spectral

response in contrast to the more dark and red reflectance typical of the rest of the surface. The lack of the 1.5 and 2.0 μm water ice absorption bands in the ubiquitous low-albedo material on 67P/CG indicates a very dehydrated surface with the water ice abundance <2% on average (Raponi et al. 2020). Crystalline water ice has been identified only on specific areas of the nucleus during the pre-perihelion phase (De Sanctis et al. 2015; Barucci et al. 2016; Filacchione et al. 2016a; Raponi et al. 2016). Also CO₂ ice has been detected for the first time on a cometary nucleus surface by VIRTIS in a small area located in the meridional Anhur region (Filacchione et al. 2016b). Note that the surface composition of 67P/CG is pristine since a continuous rejuvenation of its surface occurs during the perihelion passages. For each orbit, cometary activity erodes at least a layer of 1.0 \pm 0.5 m surface thickness (Bertaux 2015) on average, whereas Fulle et al. (2019) have estimated an erosion of about 4 m at perihelion for the southern hemisphere.

The most striking spectral feature is the broad band between 2.8 and 3.6 μm centered at 3.2 μm , whose attribution is challenging. The band falls in a spectral region where the contribution to the absorption of X–H stretching vibrations in different functional groups is expected. C–H vibrations in aliphatic and aromatic C bonding have recently been established as substructures of the observed absorption band in newly calibrated VIRTIS spectra (Raponi et al. 2020). O–H vibrational modes in water ice, structural water or chemisorbed

hydroxyl groups absorb from 2.7 to 3.1 μm but cannot explain the entire feature. Quirico et al. (2016) suggested several possibilities, OH groups in carboxylic acids inserted in a macromolecular organic solid and NH_4^+ (ammonium) ions were proposed as plausible candidates to encompass the broad width of the cometary feature. More recently on the basis of laboratory experiments, the 3.2 μm band and some of its subfeatures have been interpreted to be ammonium (NH_4^+) salts (such as ammonium formate, sulfate, citrate) mixed with dark cometary surface material (Poch et al. 2020).

Silicates, together with powders of coal and iron sulfides, have been used to model the red visible and near-infrared slope and low albedo of 67P/CG (Rousseau et al. 2018). Detection in the coma of a mineral phase, predominantly composed of silicates and carbonaceous components, was carried out by the COSIMA experiment on board Rosetta (Bardyn et al. 2017). The presence of silicates in comets was first reported by Bregman et al. (1987) and later confirmed by Campins & Ryan (1989) in comet 1/Halley and by Crovisier et al. (1997) in Hale-Bopp (C/1995 O1). During their journey from the birth sites around evolved stars through the interstellar medium (ISM) to comets, silicates interact with ions (mainly protons), which induce many effects such as amorphization, sputtering, and implantation with the formation of OH groups (Demyk et al. 2001, 2004; Carrez et al. 2002; Jäger et al. 2003a; Brucato et al. 2004; Djouadi et al. 2005). The abundance of amorphous silicates in the ISM is 98% with respect to the crystalline counterpart, whereas the abundance varies between 70% and 98% for Jupiter-family comets (Sugita et al. 2005). Furthermore, the silicates are primarily Mg-rich (e.g., Kelley et al. 2017). Direct evidence of silicate processing by ions has come from analysis of interplanetary dust particles (IDPs; Bradley 1994; Bradley et al. 1999, 2005). During their journey, silicates can also interact with hydrogen atoms both in diffuse and dense regions of the ISM.

In this Letter, we experimentally investigate the consequence of the interaction of H atoms with analogs of interstellar silicate grains. Hydrogen atoms, with an energy of a few tens of meV, form hydroxyl groups in Mg-rich amorphous silicates with different Mg/Si ratios. The resulting IR spectrum is characterized by a broad absorption band centered at 3.2 μm similar to the one observed in 67P/CG spectrum.

2. Experiments and Results

Interstellar amorphous silicate analogs were prepared by a pulsed laser ablation of targets and subsequent condensation of vapor on a polished substrate in a quenching gas atmosphere. We adopted a Nd-YAG solid state laser at the 1024 nm wavelength equipped with II and IV harmonics at 532 and 266 nm, respectively. By using a focusing lens, the power density on the target was measured by LaserMate-P power meter (Coherent) to be $1 \times 10^8 \text{ W cm}^{-2}$. The target to be ablated was mounted inside a chamber, filled with a 10 mbar Ar atmosphere, on a rotating sample holder placed in front of the laser beam. Condensed silicate vapors were collected at a distance of 5 cm from the target on ZnSe windows and carbon stubs, respectively, for IR spectroscopy and electron microscopy. We have used pellets made out of oxide mixtures in two different proportions (MgO:SiO₂ in a 1:1 and 2:1 mixture) as targets. The oxide mixtures were prepared by weighing the exact amounts of MgO (99.99%; Sigma-Aldrich) and SiO₂ (99.8%; Sigma-Aldrich) in order to have the starting

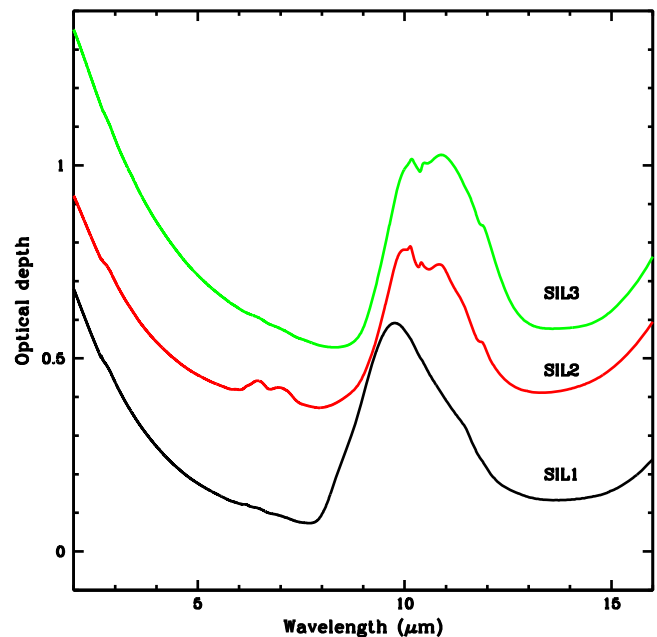


Figure 1. Infrared spectra of the silicates reported in Table 1. The spectra of SIL2 and SIL3 are offset in ordinate by 0.3 and 0.5, respectively.

Table 1
Atomic Ratios of Silicates Produced by the Laser Ablation

Sample Name	Starting Material	Measured Ratios	
		Mg/Si	Fe/Si
SIL1	MgO:SiO ₂ (1:1)	1.1	...
SIL2	MgO:SiO ₂ (2:1)	1.7	...
SIL3	Natural Olivine	1.7	0.2

stoichiometric composition of enstatite (MgSiO₃) for the first sample (SIL1) and forsterite (Mg₂SiO₄) for the second sample (SIL2). The mixtures were produced in the form of pellets (13 mm in diameter and a few millimeters in thickness) by pressing finely ground oxides at 10 tons. The third sample (SIL3) was prepared from an unpolished natural olivine rock (dunite; Webster-Addie, North Carolina, acquired from Wards Science) as the target. The three silicates (SIL1, SIL2, and SIL3) prepared in the present work are listed in Table 1. The chemical composition resulting from the process of vaporization and condensation was analyzed with an electron dispersive X-ray (EDX) system (Oxford Inca Energy 350) linked to a field emission scanning electron microscope (FESEM; ZEISS SUPRA 25). The FESEM images show that mainly a fluffy structure of amorphous grain aggregates characterizes the morphology of the silicate samples. For a detailed characterization of texture, grain dimension, and size distribution of the samples see Rotundi et al. (2000). The atomic ratio of the samples obtained by EDX is also reported in Table 1. Taking into account the variations due to nonhomogeneity of the samples, the Mg/Si ratio is in agreement with the corresponding value of the starting oxide mixtures for SIL1, while it is slightly lower in the case of SIL2. The values, Fe/Mg = 0.11 and (Mg+Fe)/Si = 1.9, indicate that the composition of the sample obtained from natural olivine (SIL3) is Mg-rich.

Figure 1 shows the optical depth of the silicates acquired with a Fourier transform infrared (FTIR) spectrometer (Bruker

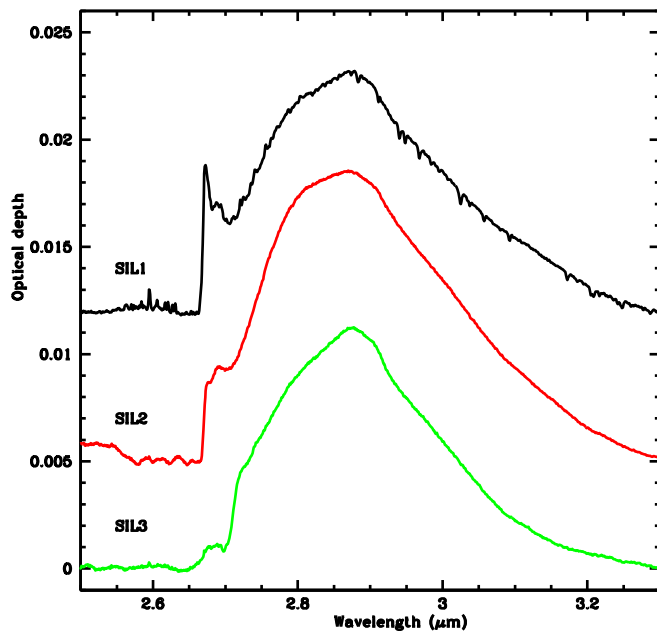


Figure 2. Infrared spectra, after continuum removal, of the silicates reported in Table 1 in the 2.5–3.3 μm range. The spectra of SIL2 and SIL1 are offset in ordinate by 0.006 and 0.012, respectively.

Equinox 55). Transmittance spectra, normalized with the corresponding blank ZnSe window, were acquired in air at room temperature, in the range 2–16 μm at a spectral resolution of 2 cm^{-1} . The spectra are characterized by a strong band around 10 μm due to the Si–O stretching mode, whose profile slightly varies with the sample composition. The band is centered at 9.8 μm for SIL1 and it shifts to 10.2 μm as the Mg/Si ratio increases (for SIL2 and SIL3 samples). In the latter cases, an additional band at around 10.8 μm is also evident. Jäger et al. (2003b) also reported a similar redshift in the band position with increasing MgO/SiO₂ ratio in their amorphous magnesium silicate samples, prepared by the sol-gel method. The absorption increase for wavelengths longer than 13 μm is due to the low-energy wing of the Si–O bending feature at around 20 μm , while the increase at high energy (<7 μm) is attributed to the scattering by micron-sized particles present in the sample. The small double band at 6.5 and 7 μm , more intense in the case of SIL2, is caused by traces of magnesium carbonate, formed during sample preparation (Jäger et al. 2003b). Figure 2 shows the silicate infrared spectra in the 3 μm spectral range after continuum removal. A broad band centered at 2.88 μm , produced by adsorbed water and chemisorbed hydroxyl groups, due to ambient contamination during the sample handling at the time of pellet preparation and also at the time of laser ablation, characterizes this region. Two narrow bands at 2.67 μm and 2.69 μm are respectively attributed to isolated Si–OH and Si–H groups (Iler 1979; Shinoda et al. 2002). Their relative intensity varies according to the Mg/Si ratio. In the case of SIL3, produced from natural olivine, only a weak band, resulting from the blend of the two features, is observed. Similar bands have been detected in silicates produced by the sol-gel method (Jäger et al. 2003b), suggesting that laser ablation and sol-gel techniques provide materials that are good analogs for cosmic silicates. In fact, the formation of silicates in space with a small content of isolated Si–OH and Si–H bonds can be considered highly probable, since H₂O, the

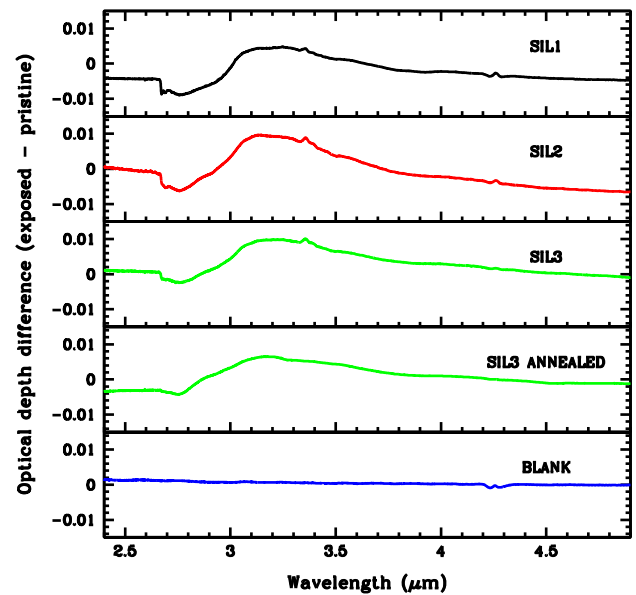


Figure 3. Spectral changes of silicates under exposure (shown after subtraction of the initial spectrum) of 1×10^{18} H atoms cm^{-2} . The spectrum of a ZnSe window (blank) after the same exposure is also reported for comparison. The feature at around 4.25 μm is associated with uncompensated ambient CO₂.

most abundant oxygen-bearing molecule, participates in the formation of olivine and pyroxene-type silicates around evolved stars (Gail & Sedlmayr 1998; Jäger et al. 2003b).

To study the interaction of hydrogen with silicates, our samples were placed inside a vacuum chamber, with a base pressure of 2×10^{-8} mbar, on a rotating sample holder at the right angle intersection between an atomic hydrogen beam and the IR beam of an FTIR spectrophotometer (Bruker Vertex 80). H atoms were produced by microwave dissociation of molecular hydrogen; they have a Maxwellian velocity distribution at 300 K (Mennella 2006). After H atom exposure, the sample was rotated by 90° to face the IR beam, and we measured the IR spectrum with a resolution of 2 cm^{-1} in the range 2–5 μm (5000–2000 cm^{-1}). The IR background was acquired before each spectra by removing the sample holder from the beam path using a micromanipulator. Figure 3 shows the spectral changes, obtained by subtracting the pre-exposed spectrum from the exposed one, induced by H atom exposure in amorphous silicates. The activation of a broad band centered at about 3.2 μm takes place in all the silicates. At shorter wavelengths, an absorbance decrease in the exposed sample (resulting in a negative optical depth difference in Figure 3) centered at 2.76 μm (broad band) and bands at 2.67 and 2.69 μm (sharp doublet) are observed. This behavior indicates that the H atoms induced a depletion of the O–H bonds already present in the starting silicate samples.

In addition, a weak feature at 3.36 μm with a shoulder at 3.39 μm is possibly due to asymmetric C–H stretching modes of aliphatic CH₃ and CH₂ groups. They could have originated from the processing of carbonate and other atmospheric contaminants present in the sample. The faint feature at around 4.25 μm is associated with uncompensated ambient CO₂. Exposure of a blank ZnSe substrate to hydrogen (see Figure 3) does not induce any variation in the spectrum, demonstrating that the observed spectral changes are due to the interaction of hydrogen with silicate grains.

To investigate whether the presence of OH groups in the pristine silicates affects their interaction with hydrogen, we tried to eliminate/reduce them by annealing one of the samples (SIL3) at 300°C for 1 hr before exposure to H atoms. In the case of the annealed SIL3, only a small absorbance decrease centered at 2.76 μm is present after exposure to hydrogen atoms (see Figure 3), testifying that the starting sample was almost fully depleted of the chemisorbed hydroxyl groups. Despite that, the activation of the 3.2 μm band does not vary. Hydroxylation of Mg-rich amorphous silicates by H atoms is therefore independent of the OH groups already present in silicates and of the specific composition of the samples.

3. Discussion and Conclusions

The spectral variations induced in Mg-rich silicates by atomic hydrogen are clear evidence for chemical reactions producing hydroxyl groups on silicates. According to density functional quantum mechanical calculations, the formation of OH groups in Mg-rich silicate nanoclusters by impinging H atoms takes place without any significant energy barrier (Kerkeni et al. 2017). The observed spectral evolution with H atom exposure suggests that hydroxyl groups are formed by hydrogen atom interaction on surface of amorphous silicates, which have a wide range of binding sites enhancing both physisorption and chemisorption of hydrogen. The nature (distribution of sites and chemical state) of our samples determines the observed broad band. The spectral changes indicate that exchange reactions (addition and abstraction of H atoms in OH) are active during H atom exposure of our samples. Once an H atom forms an OH group on an available site (addition reaction), a second impinging H atom can abstract it, forming H_2 (abstraction reaction). This leaves a site available to form again a hydroxyl group when a third atom arrives. The equilibrium value for the number of OH groups after H atom exposure depends on the cross section of the abstraction and addition process. The observed absorbance decrease at 2.76 μm (broad band) and at 2.67, 2.69 μm (sharp doublet) indicates a reduction in the number of OH bonds (already present in the samples) since their initial value was higher than the equilibrium value. On the other hand, the absorbance increase at longer wavelengths corresponds to an increase of the number of OH groups, initially absent in the sample.

Formation of OH bonds with a peak at around 2.8 μm has been reported after implantation of keV to MeV energy range protons in silicates with different composition and structure (e.g., Zeller et al. 1966; Djouadi et al. 2011; Schaible & Baragiola 2014). Exchange of H/D in hydroxyl groups has also been observed after 1.1 keV D^+ implantation of Apollo lunar soils (Ichimura et al. 2012). Hydroxylated silicates produced by proton implantation have also been considered as a potential reservoir of water during the formation of terrestrial planets (Djouadi et al. 2011). So far, it has been believed that hydroxylation of silicates occurred by high-energy proton implantation on the surface of airless solar system bodies such as the Moon. Our experiments show that the process can also take place when low-energy (a few tens of meV) H atoms interact with amorphous silicate grains. This can happen in the ISM where both atomic hydrogen and amorphous silicate grains are present.

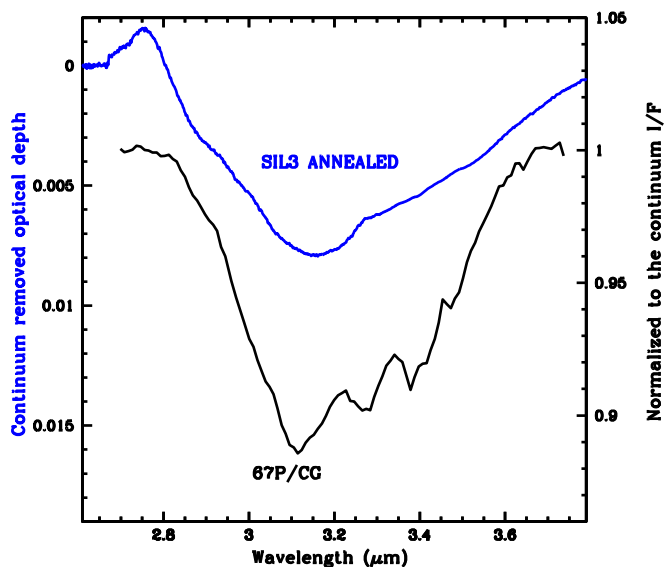


Figure 4. Qualitative comparison of 3.2 μm absorption band in SIL3 (blue line) first annealed at 300°C and then exposed to 1×10^{18} H atoms cm^{-2} to the observed absorption band in the 67P/CG reflectance spectrum (black line). The left vertical axis is for the SIL3 spectrum, whereas the right vertical axis refers to that of the cometary band.

There is a clear difference in the width and peak position of the OH IR band in the two interactions. As shown in the present experiments, the band is centered at longer wavelengths, and it is much wider than that obtained by proton implantation. The origin of the observed differences is the distribution of sites and chemical state of the samples studied in the two cases. To get further insight, besides IR spectroscopy, other analytical techniques such as X-ray photoelectron spectroscopy (XPS) would be useful to understand the difference in the chemical state of the oxygen atoms present in the sample. In addition, high-energy proton implantation on our amorphous silicate grains will also be essential to compare the effects induced by the two processes.

The profile of the band formed by H atoms in the considered silicates (see Figure 3) is reminiscent of the 3.2 μm absorption band in the reflectance spectrum of 67P/CG observed by VIRTIS on board Rosetta (Raponi et al. 2020). Figure 4 shows the comparison of the cometary profile with that of annealed SIL3. The similarity in profile suggests that OH groups of hydroxylated amorphous silicates can be a constituent of the 67P/CG nucleus surface, together with aliphatic carbons, ammonium salts, water ice, and possibly polycyclic aromatic hydrocarbons (Quirico et al. 2016; Poch et al. 2020; Raponi et al. 2020).

To quantitatively evaluate the spectral contribution of hydroxylated amorphous silicate to the 3.2 μm band, we have modeled the average reflectance (I/F) spectrum of the comet 67P/CG surface with a similar approach already used to estimate the spectral contribution of water ice (Raponi et al. 2020). The Hapke radiative transfer model (Hapke 2012) was adopted to calculate the reflectance of an intimate mixture of hydroxylated amorphous silicate with a synthetic continuum representing a dark-red terrain. Model fits to the average 67P/CG reflectance spectrum indicate that hydroxylated silicate can reproduce on average 65% of the 3.2 μm cometary band intensity with an abundance of hydroxylated amorphous

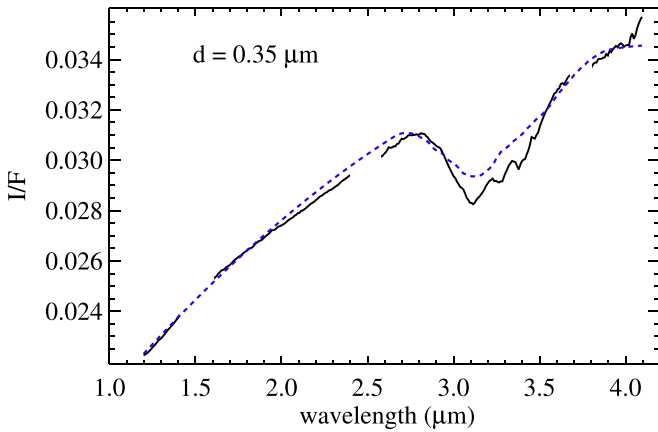


Figure 5. Fit to the average 67P/CG reflectance spectrum (black line; Raponi et al. 2020) by the modeled hydroxylated amorphous silicate mixed with the dark-red end-member (blue dashed line) using Hapke’s model for $5 \mu\text{m}$ grain size and 15% of hydroxylated amorphous silicate abundance. See the Appendix for the meaning of d and other parameters.

silicate of 15%. An example of the resulting modeling is shown in Figure 5 (for more details see the Appendix). The estimated contribution should be considered as an upper limit due to the involved assumptions. It is worth stressing that for an accurate quantitative estimation, one should also consider the contributions of the other proposed carriers of the $3.2 \mu\text{m}$ band as mentioned above.

The presence of a hydroxylated fraction in silicates on the surface of a comet can represent an evolutionary link between a primitive object of the solar system and dust in the ISM. The spectral homogeneity of the nucleus surface observed by VIRTIS indicates that the composition of the refractory surface materials does not change despite the rejuvenating processes active during the perihelion passages of 67P/CG (Ciarniello et al. 2016). The refractory material seen at the surface must be then representative of the bulk pristine material of the nucleus. As for all cosmic dust, silicates participate in the life cycle of matter that brings dust from their circumstellar birth sites to the diffuse interstellar medium and dense clouds where stars form. The formation of planetary systems, like our solar system, can also take place during this cycle. Since silicates are involved in the global evolution of the interstellar matter, from diffuse medium to comets, they interact with hydrogen atoms in the ISM. The laboratory H atom fluence of 1×10^{18} atoms cm^{-2} used in the present experiments as reported in Figure 3 corresponds to an H atom exposure time of 4×10^3 and 4×10^5 yr, respectively, in interstellar diffuse and dense regions (considering the respective H atom flux of 8×10^6 and 9×10^4 atoms $\text{s}^{-1} \text{cm}^{-2}$ for these regions; Mennella 2010). In addition, we observed the formation of the $3.2 \mu\text{m}$ band already at a lower fluence of $\sim 10^{16}$ atoms cm^{-2} . Therefore, hydroxylation can take place on a much shorter timescale compared to the residence time of 3×10^7 yr of dust grains in both dense and diffuse regions of the ISM. Note that, although the silicate hydroxylation experiments were performed at 300 K, the results maintain their relevance for low-temperature interstellar conditions since the reaction should occur without a significant energy barrier (see the first paragraph of this section). However, for an accurate evaluation of the silicate hydroxylation degree in different regions of the ISM, we also need to know the hydroxylation cross section as well as the

effects of the dehydrogenation processes induced by UV photons and cosmic rays.

The evolutionary link suggested by the present results is consistent with the detection of the aliphatic matter in 67P/CG (Raponi et al. 2020). We thus can trace for both aliphatic carbon and hydroxylated amorphous silicates a common origin in the ISM during the journey of the dust from its birth sites around evolved stars to our solar system.

This work is supported by the International Space Science Institute (ISSI) through the collaboration of the ISSI international team “Comet 67P/Churyumov–Gerasimenko Surface Composition as a Playground for Radiative Transfer Modelling and Laboratory Measurements,” number 397.

Appendix

Modeling of the Spectral Contribution of Hydroxylated Silicates to the $3.2 \mu\text{m}$ Feature of 67P/CG

We apply the Hapke model (Hapke 2012) to derive an upper limit of the amount of hydroxylated Mg-rich amorphous silicates contributing to the $3.2 \mu\text{m}$ band intensity of 67P/CG (Raponi et al. 2020). To this aim, 67P/CG’s surface is modeled as an intimate mixture of a featureless dark-red synthetic component, representing predominantly the optically opaque phases in the comet regolith, and a hydroxylated Mg-rich amorphous silicate. The spectral output of the featureless end-member is modeled as a continuum by means of a second-degree polynomial, while for the hydroxylated Mg-rich amorphous silicate material, synthetic optical constants have been computed. Upon exposure to H atoms, the optical properties of the amorphous silicates are modified by formation of the absorption feature centered at $3.2 \mu\text{m}$. This effect can be interpreted as an increase of the value of the imaginary part of the refractive index k , Δk , in correspondence to the $3.2 \mu\text{m}$ absorption feature. To estimate Δk , we represent the contribution of OH groups formed on the fluffy and amorphous grain aggregates in consideration by assuming a homogenous film of hydroxylated amorphous silicate of equivalent thickness d . Then the measured optical depth difference (exposed-pristine) can be expressed as

$$\Delta\tau(\lambda) = \frac{4\pi}{\lambda} d \Delta k. \quad (\text{A1})$$

The equivalent thickness d can be derived from the integrated optical depth through the following relation:

$$\int_{\text{band}} \Delta\tau(\nu) d\nu = NA = \frac{\rho d N_A}{m} A, \quad (\text{A2})$$

where N is the column density, A is the integrated band strength, and N_A is Avogadro’s number. ρ and m are the density and the molecular weight of the film, respectively. We evaluated the integral in the left-hand term of Equation (A2) from the annealed SIL3 reported in Figure A1 and adopt $A = 2 \times 10^{-17}$ cm molecule^{-1} , as in the case of the OH groups in natural olivine (Schaible & Baragiola 2014). Moreover, we assumed $\rho = 1 \text{ g cm}^{-3}$ and $m = 101 \text{ g mol}^{-1}$ for hydroxylated silicate film with a starting silicate stoichiometry as $[\text{MgO.SiO}_2]$. We obtain a starting value of $d = 0.35 \mu\text{m}$. It is then possible to derive the corresponding increase of the imaginary part of the refractive index from Equation (A1) as

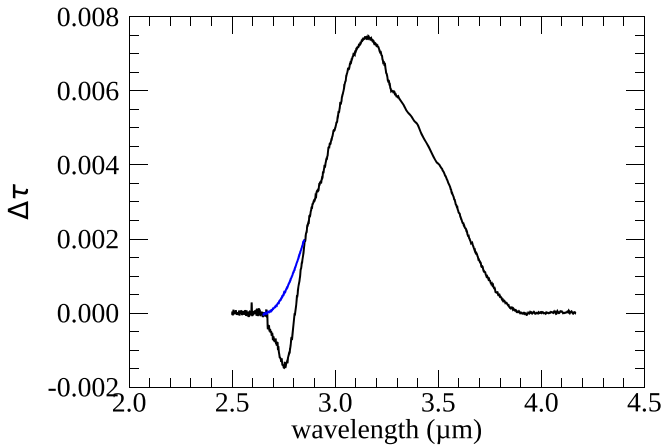


Figure A1. Optical depth difference (after continuum removal) for annealed SIL3. As mentioned in the text, the H atom interaction results in abstraction of H atoms in OH groups already present in the sample, introducing a spurious negative signature in the $\Delta\tau$ spectrum between 2.65 and 2.85 μm . To eliminate this spurious signature, we discard the measurement in this range and replace it by a polynomial (blue segment) that connects the part of the optical depth difference spectrum shortward of 2.65 μm with the region longward of 2.85 μm .

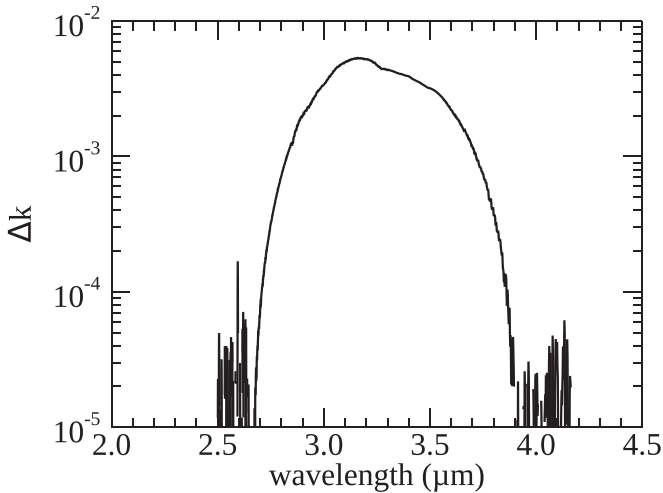


Figure A2. Δk as a function of wavelength for $d = 0.35 \mu\text{m}$.

seen in Figure A2. To see how the final results are affected by our assumptions, we also varied d by a factor of 10 higher and lower, reflecting possible uncertainties in the assumptions on A , ρ , and m .

Since the H atom processing of Mg-rich amorphous silicates does not lead to variations of the absorption spectrum outside the 3.2 μm band, it is reasonable to assume the imaginary part of the refractive index k_b of the unprocessed silicate as a baseline. However, optical constant values of the unprocessed silicates analyzed in the present work are missing. Therefore, we adopted the optical constants of similar silicates. The choice is further justified by the fact that H atom interaction modifies different Mg-rich amorphous silicates in a similar way, as also evidenced by the reported measurements. We considered real and imaginary parts of optical constants of Mg-rich glass from Dorschner et al. (1995). Further, to incorporate the effects of H atom processing on the optical constants, a synthetic imaginary

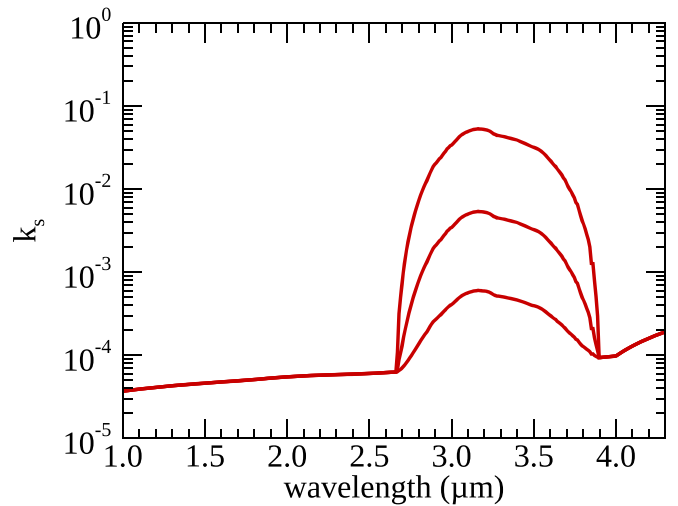


Figure A3. Imaginary part of the synthetic refractive index derived by using Mg-rich glass as the baseline. The three curves represent the different values of k_s obtained for d values of 0.035, 0.35, and 3.5 μm from top to bottom, respectively.

part of the refractive index $k_s = k_b + \Delta k$ is derived as shown in Figure A3, for the Mg-rich glass for different values of d .

For each synthetic refractive index values, a fit to the 67P/CG spectrum is performed in a similar way as Raponi et al. (2020) did for water ice. We forced the fit to match the continuum level of the cometary spectrum in the range between 2.7–2.9 μm and 3.5–3.6 μm to ensure that the modeled absorption is not more intense than the one shown by 67P/CG. The best fits to the 67P/CG spectrum are reported in Figure A4, while the best-fit parameters, i.e., the hydroxylated silicate abundance, R , and the corresponding grain size, S , are listed in Table A1. Note that R values reported in Table A1 represent the corresponding fractional cross section seen by the light propagating within the medium. These quantities can be interpreted as volumetric abundances under the assumption that the featureless dark-red terrain has the same grain size as the hydroxylated silicate. The derived R values are constant at 0.15, and F is very similar for the three cases with an average value of around 0.65. Conversely, the obtained S values increase with d . This can be explained by the fact that Δk as obtained from Equation (A1) is lower for larger d , thus producing a smaller absorption for a given grain size. Given this, in order to reproduce the observed spectral contrast, a larger value of S is required in the modeling. One should note that a rigorous application of the Hapke's model would limit its application to the geometric optics regime, where particles are larger than wavelength. This is the case for the derived value of $S = 0.5 \mu\text{m}$, which implies that small particle sizes (likely sub- μm) are required to match the observed spectrum with the adopted set of optical constants.

The estimated abundance of 15% of hydroxylated silicates (see R in Table A1) is in good agreement with previous results obtained by Rousseau et al. (2018). They have reproduced the reflectance spectra of the cometary nucleus of 67P/CG using mixtures of silicate and dark materials (coal and sulfide) where the silicate fraction was estimated to be <30% (weight%) with respect to the total mixture. Assuming the density of the silicates as 3 g cm^{-3} , and the average density of the dark

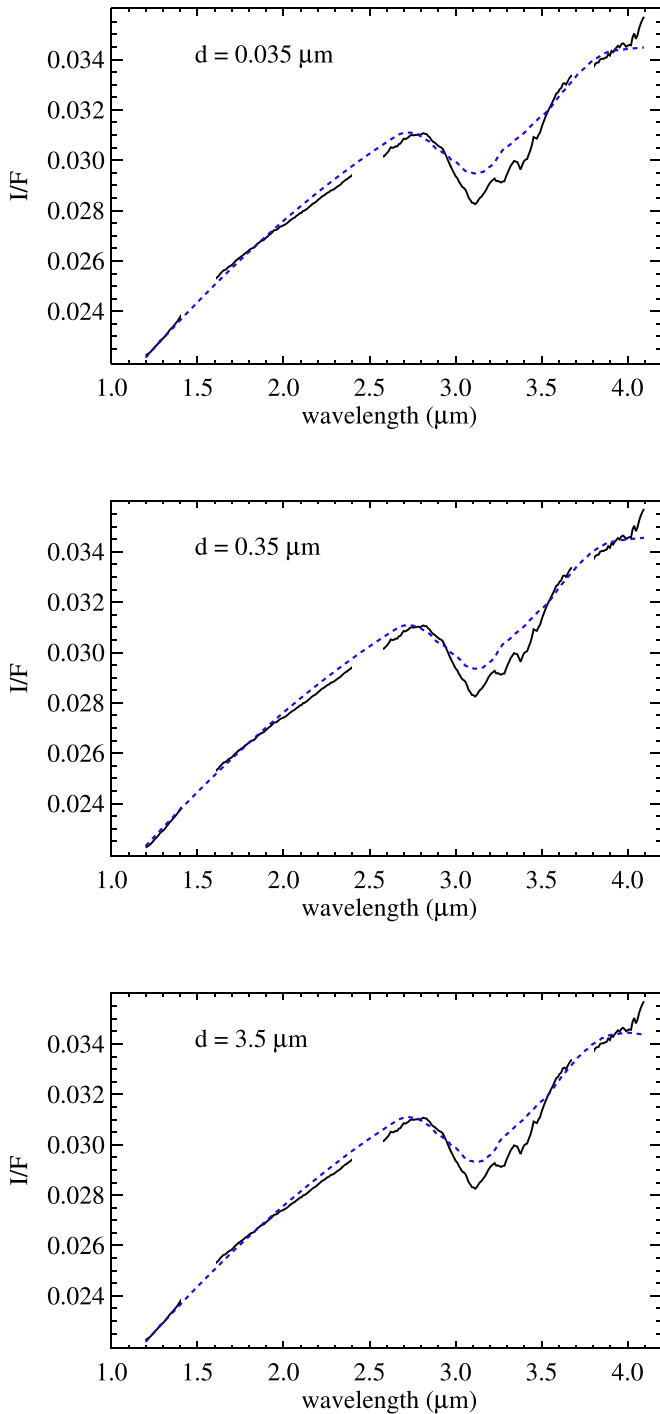


Figure A4. From top to bottom: best fits (blue dashed lines) to average 67P/CG reflectance spectrum (black lines) obtained with synthetic optical constants computed using Mg-rich glass (Dorschner et al. 1995) as the baseline for different values of d .

Table A1

Best-fit Parameters (R , S) of the Model to the Average Reflectance Spectrum of 67P/CG

Equivalent Film	Hydroxylated Silicate	Grain Size	Fraction of the 3.2 μm Band Intensity Due to Hydroxylated Silicates
Thickness d μm	Abundance R	S μm	F
0.035	0.15	0.5	0.62
0.35	0.15	5	0.66
3.5	0.15	50	0.67

components as 2 g cm^{-3} , a volumetric silicate abundance of 20% is obtained. In addition, our result leaves enough room for other darkening agents that can justify the observed low albedo.

ORCID iDs

V. Mennella <https://orcid.org/0000-0001-9525-895X>
M. Ciarniello <https://orcid.org/0000-0002-7498-5207>
A. Raponi <https://orcid.org/0000-0003-4996-0099>
G. Filacchione <https://orcid.org/0000-0001-9567-0055>
D. Kappel <https://orcid.org/0000-0002-0518-5548>
V. Vinogradoff <https://orcid.org/0000-0003-4107-0980>
C. Pilorget <https://orcid.org/0000-0002-7759-9854>

References

- Bardyn, A., Baklouti, D., Cottin, H., et al. 2017, *MNRAS*, 469, S712
Barucci, M. A., Filacchione, G., Fornasier, S., et al. 2016, *A&A*, 595, A102
Bertaux, J.-L. 2015, *A&A*, 583, A38
Bradley, J., Dai, Z. R., Erni, R., et al. 2005, *Sci*, 307, 244
Bradley, J. P. 1994, *Sci*, 265, 925
Bradley, J. P., Keller, L. P., Snow, T. P., et al. 1999, *Sci*, 285, 1716
Bregman, J., Campins, H., Witteborn, F., et al. 1987, *A&A*, 187, 616
Brucato, J. R., Strazzulla, G., Baratta, G., & Colangeli, L. 2004, *A&A*, 413, 395
Campins, H., & Ryan, E. V. 1989, *ApJ*, 341, 1059
Capaccioni, F. a., Coradini, A., Filacchione, G., et al. 2015, *Sci*, 347, aaa0628
Carrez, P., Demyk, K., Cordier, P., et al. 2002, *M&PS*, 37, 1599
Ciarniello, M., Capaccioni, F., Filacchione, G., et al. 2015, *A&A*, 583, A31
Ciarniello, M., Raponi, A., Capaccioni, F., et al. 2016, *MNRAS*, 462, S443
Coradini, A., Capaccioni, F., Drossart, P., et al. 2007, *SSRv*, 128, 529
Crovisier, J., Leech, K., Bockelee-Morvan, D., et al. 1997, *Sci*, 275, 1904
De Sanctis, M. C., Capaccioni, F., Ciarniello, M., et al. 2015, *Natur*, 525, 500
Demyk, K., Carrez, P., Leroux, H., et al. 2001, *A&A*, 368, L38
Demyk, K., d'Hendecourt, L., Leroux, H., Jones, A., & Borg, J. 2004, *A&A*, 420, 233
Djouadi, Z., d'Hendecourt, L., Leroux, H., et al. 2005, *A&A*, 440, 179
Djouadi, Z., Robert, F., d'Hendecourt, L. L. S., et al. 2011, *A&A*, 531, A96
Dorschner, J., Begemann, B., Henning, T., Jaeger, C., & Mutschke, H. 1995, *A&A*, 300, 503
Filacchione, G., De Sanctis, M., Capaccioni, F., et al. 2016a, *Natur*, 529, 368
Filacchione, G., Groussin, O., Herny, C., et al. 2019, *SSRv*, 215, 19
Filacchione, G., Raponi, A., Capaccioni, F., et al. 2016b, *Sci*, 354, 1563
Fulle, M., Blum, J., Green, S., et al. 2019, *MNRAS*, 482, 3326

- Gail, H.-P., & Sedlmayr, E. 1998, in *The Molecular Astrophysics of Stars and Galaxies*, ed. T. W. Hartquist & D. A. Williams (Oxford: Clarendon), 285
- Hapke, B. 2012, *Theory of Reflectance and Emittance Spectroscopy* (Cambridge: Cambridge Univ. Press)
- Ichimura, A., Zent, A., Quinn, R., Sanchez, M., & Taylor, L. 2012, *E&PSL*, 345, 90
- Iler, K. R. 1979, *The Chemistry of Silica* (New York: Wiley)
- Jäger, C., Dorschner, J., & Mutschke, H. 2003a, *A&A*, 408, 193
- Jäger, C., Fabian, D., Schrepel, F., et al. 2003b, *A&A*, 401, 57
- Kelley, M. S., Woodward, C. E., Gehr, R. D., Reach, W. T., & Harker, D. E. 2017, *Icar*, 284, 344
- Kerkeni, B., Bacchus-Montabonel, M.-C., & Bromley, S. T. 2017, *MolAs*, 7, 1
- Mennella, V. 2006, *ApJL*, 647, L49
- Mennella, V. 2010, *ApJ*, 718, 867
- Poch, O., Istiqomah, I., Quirico, E., et al. 2020, *Sci*, 367, eaaw7462
- Quirico, E., Moroz, L., Schmitt, B., et al. 2016, *Icar*, 272, 32
- Raponi, A., Ciarniello, M., Capaccioni, F., et al. 2016, *MNRAS*, 462, S476
- Raponi, A., Ciarniello, M., Capaccioni, F., et al. 2020, *NatAs*, 4, 500
- Rotundi, A., Rietmeijer, F., Brucato, J., et al. 2000, *P&SS*, 48, 371
- Rousseau, B., Érard, S., Beck, P., et al. 2018, *Icar*, 306, 306
- Schaible, M. J., & Baragiola, R. A. 2014, *JGRE*, 119, 2017
- Shinoda, K., Yamakata, M., Nanba, T., et al. 2002, *PCM*, 29, 396
- Sugita, S., Ootsubo, T., Kadono, T., et al. 2005, *Sci*, 310, 274
- Taylor, M., Altobelli, N., Buratti, B., & Choukroun, M. 2017, *RSPTA*, 375, 20160262
- Zeller, E. J., Ronca, L. B., & Levy, P. 1966, *JGR*, 71, 4855